

# $\pi N \rightarrow \eta N$ and $\eta N \rightarrow \eta N$ partial wave T-matrices in a coupled, three channel model

Mijo Batinić, Ivo Šlaus, Alfred Švarc  
*Ruđer Bošković Institute, Zagreb, Croatia*

and

B.M.K. Nefkens  
*University of California Los Angeles*  
*USA*

The  $\pi N \rightarrow \eta N$  and  $\eta N \rightarrow \eta N$  partial wave T-matrices for the eight lowest partial waves have been obtained in a three coupled channel model with unitarity manifestly imposed. The two physical channels are  $\pi N$  and  $\eta N$ , and the third channel,  $\pi\pi N$  is an effective, but unphysical two body channel which represents all remaining processes. The  $\pi N$  elastic phase shifts and the weighted data base of the  $\pi N \rightarrow \eta N$  total and differential cross sections are chosen as the input for the fitting procedure. A model containing a single resonance in each of the three partial waves that dominates the  $\eta$  production at lower energies is compared with previous analyses, based on similar assumptions. A multiresonance coupled channel model is introduced which significantly improves the agreement with all input data. Our results are compared with a complementary multiresonance coupled channel analysis that is constrained with elastic and continuum production channels. The inclusion of the fourth  $P_{11}$  resonance in the 1440 - 2200 MeV region further improves the agreement between the analysis and the data.

## I. INTRODUCTION

The cross section for  $\eta$ -meson production by pions

$$\pi^- p \rightarrow \eta n \tag{1}$$

has a large peak at an energy close to the  $\eta$  production threshold, see Figs. 1a and 1b. The maximum value,  $\sigma_{tot}(\pi^- p \rightarrow \eta n) = 2.8$  mb, is 6 % of  $\sigma_{tot}(\pi^- p \rightarrow \text{all})$  [1]. This large peak is usually associated with the  $S_{11}(1535)$  isobar known from  $\pi N$  elastic scattering and photoproduction. Recently, Höhler [2] has drawn attention to a peculiar feature of this  $S_{11}$  resonance, namely, that the speed plot analysis of S-wave  $\pi N$  scattering has a sharp spike at the opening of the  $\eta$  channel and no clear, independent indication of a resonance in the energy region around 1535 MeV. This suggests a strong interplay between the cusp associated with the opening of the  $\eta$  channel and the excitation of the  $S_{11}$  resonance.

Some time ago Bhalerao and Liu [3] analyzed the then available  $\pi N \rightarrow \eta N$  data in a coupled-channel, single resonance separable interaction model in which the reaction proceeds via the formation of  $\Delta$  and  $N^*$  isobars - and concluded that the S-wave  $\eta N$  interaction is attractive. They found the value of the S-wave scattering length of  $a_{\eta N} = (0.27 + i 0.22)$  fm. Arima et al [4] obtained  $a_{\eta N} = (0.98 + i 0.37)$  fm, while Wilkin, based on an S-wave threshold enhancement calculation, quotes the value of  $a_{\eta N} = (0.55 \pm 0.20 + i 0.30)$  fm [5]. The large spread in these values of the fundamental  $a_{\eta N}$  parameter illustrates the need for better understanding of the  $\eta N$  system at low energies. The first step to do this is to obtain a reliable set of  $\pi N \rightarrow \eta N$  T-matrices.

The indication of strong and attractive  $\eta N$  interaction has led to a speculation about the existence of a new type of nuclear matter, namely, quasi-bound  $\eta$ -mesic nuclei [6]. The properties of this new matter are determined by the  $\eta N$  interaction at low energies.

Good data on  $\eta$  production in  $\pi^- p$  interaction is missing. The dominant contribution to the surprisingly big  $\eta$  production channel is coming from the  $S_{11}(1535)$  resonance, the contribution of the  $P_{11}(1440)$  and  $D_{13}(1520)$  resonances is important, but not completely clarified. The role of other resonances, even in these partial waves, is not at all discussed because of the single resonance character of the model. Recently, accurate  $\eta$  photoproduction data have been obtained by TAPS at MAMI

[7] up to  $E_\gamma = 790$  MeV. These data indicate that the  $D_{13}$  resonance contribution is small.

The objective of this paper is to furnish a set of  $\pi N \rightarrow \eta N$  partial wave T matrices that describe the available data in a straightforward way. It is essential to get reliable information on  $\pi N \rightarrow \eta N$  on shell T matrices to be able to calculate the higher order processes where the  $\eta$  production vertex is a part of the higher order diagram, for instance in  $pp \rightarrow pp\eta$ . Several publications, dealing with higher order processes, have either used the dominant  $S_{11}$  partial wave [8–10] or have included other partial waves [3,11] for obtaining the elementary  $\pi N \rightarrow \eta N$  amplitudes. It is clear from Fig. 1a and 1b, where a comparison of different model predictions with experimental data is given, that only one s-wave resonance is not sufficient, the  $S_{11}(1535)$  resonance accounts only for the part of the  $\eta$  production total cross section, for the energy range of the  $S_{11}(1535)$  dominance. A single resonance model for the s-wave only is, therefore, incapable of describing all of  $\eta$  production data, but it may suffice for the region of the  $S_{11}(1535)$  dominance, which corresponds to  $p_\pi$  less than 850 MeV/c. To set the stage, we have tested a simple single resonance model for all three dominant partial waves;  $S_{11}$ ,  $P_{11}$  and  $D_{13}$  without any background terms added. The model describes the large near threshold peak, but it fails miserably in comparison with data above  $T_\pi = 800$  MeV. The recent single resonance model by Bennhold and Tanabe (B-T) [12] is, anyhow, limited to  $T_\pi$  less than 700 MeV. It describes the dominant peak pretty well on the gross scale, but significantly fails in giving details like the exact peak position, etc. (see Fig. 1b). The reason for the failure is that the B-T analysis relies on the data of Ref. [13], which suffer from a serious beam momentum calibration error [14]. We have also used data of Ref. [13], but with caution, as elaborated in detail later in the text. The comparison between the two models is shown in Fig. 1a and in the expanded scale in Fig. 1b. Considering that the model of B-T [12] used erroneous data of Ref. [13] and has an energy dependent form factor, which is not included in our study, the agreement between the predictions of our single resonance model and the B-T model, is satisfactory. Of course, both single resonance models miserably fail to fit the data above 800 MeV.

To obtain a better description of the input data we propose a multiresonance coupled channel model with a smooth background added in a unitary way [15] similar as in the Karlsruhe-Helsinki partial wave analysis (K-H PWA) of  $\pi N$  elastic scattering [16]. A data base consisting of  $\pi N$  K-H PWA of Ref. [16], with the addition of total

and differential  $\pi N \rightarrow \eta N$  cross sections [1,13,17–23] has been chosen in order to perform the fitting procedure of the  $\pi N$  elastic partial waves up to  $T_\pi = 2727$  MeV with the additional weighting factors based on the analyses of the data reliability by Clajus and Nefkens [14]. Results for the obtained resonance parameters slightly deviate from the  $\pi N$  elastic case, but they give acceptable  $\pi N \rightarrow \eta N$  partial wave T-matrices and at the same time predict the T matrices for the  $\eta N$  elastic process. Manley and Salesky (M-S) [24] have used a multichannel and multiresonance K-matrix approach to the coupled channel inelastic  $\pi N$  scattering with the main inelastic channel being the continuum production. The  $\eta$  production process is only added in two partial waves, the  $S_{11}$  and  $F_{17}$ . The only purpose for including the  $\eta$  production channel is to maintain unitarity when the observed loss of flux can not be attributed to any other process. The so called "  $\eta$  production channel" have to account for ALL missing inelasticity within the partial wave and cannot be related just to  $\eta$  production. Therefore, the prediction for the two  $\eta$  production partial waves T-matrices  $S_{11}$  and  $F_{17}$ , which come from the M-S model [24,25] should be used with care. As the complete study of the  $\eta$  production process requires all partial waves we have made a multiresonance three coupled channel fit with the  $\eta N$  channel explicitly included and used as a constraint. The multiresonance M-S model [24,25] is complementary to ours in the sense that our results for the resonance branching ratios for the  $\pi^2 N$  channel can be compared to the continuum production branching ratios in M-S model, and they should (but only roughly) correspond.

## II. FORMULATION OF THE MODEL

### A. The three body coupled channel formalism

The  $\pi N \rightarrow \eta N$  process is given by the invariant amplitude  $A(W, \cos \theta^*) + \not{q}_\eta B(W, \cos \theta^*)$

with the standard on-shell partial waves decomposition of  $A$  and  $B$ :

$$A(W, \cos \theta^*) = \frac{4\pi}{\sqrt{q_\pi^{*3} q_\eta^{*3}}} \left\{ \sum_{l=0}^{\infty} T_{l+} \left[ \sqrt{(E_i^* + m)(E_f^* + m)}(W - m) P'_l(\cos \theta^*) \right. \right. \\ \left. \left. + \sqrt{(E_i^* - m)(E_f^* - m)}(W + m) P'_{l+1}(\cos \theta^*) \right] \right\}$$

$$\begin{aligned}
& - \sum_{l=1}^{\infty} T_{l-} \left[ \sqrt{(E_i^* + m)(E_f^* + m)}(W - m)P'_{l+1}(\cos \theta^*) \right. \\
& \quad \left. + \sqrt{(E_i^* - m)(E_f^* - m)}(W + m)P'_l(\cos \theta^*) \right] \Big\} \\
& \qquad \qquad \qquad (2) \\
B(W, \cos \theta^*) = & \frac{4\pi}{\sqrt{q_\pi^* q_\eta^*}} \left\{ - \sum_{l=0}^{\infty} T_{l+} \left[ \sqrt{(E_i^* + m)(E_f^* + m)}P'_l(\cos \theta^*) \right. \right. \\
& - \sqrt{(E_i^* - m)(E_f^* - m)}P'_{l+1}(\cos \theta^*) \Big] \\
& + \sum_{l=1}^{\infty} T_{l-} \left[ \sqrt{(E_i^* + m)(E_f^* + m)}P'_{l+1}(\cos \theta^*) \right. \\
& \quad \left. \left. - \sqrt{(E_i^* - m)(E_f^* - m)}P'_l(\cos \theta^*) \right] \right\}.
\end{aligned}$$

$W$  is the total c.m. energy,

$\theta^*$  is the c.m. scattering angle,

$q_\pi^*$  and  $q_\eta^*$  are the initial pion and final  $\eta$  c.m. momenta,

$E_i^*$  and  $E_f^*$  are the initial and final nucleon c.m. energies,

$P'_l(z)$  are derivatives of Legendre polynomials,

$T_{l\pm}$  are the  $\pi N \rightarrow \eta N$  T-matrices,

and  $m$  is the nucleon mass.

The  $\pi N \rightarrow \eta N$   $T_{l+,l-}$  matrices are matrix elements of the three channel partial wave  $T^{JL}$  matrix which is given as:

$$T^{JL} = \begin{pmatrix} T_{\pi\pi}^{JL} & T_{\pi\eta}^{JL} & T_{\pi\pi^2}^{JL} \\ T_{\eta\pi}^{JL} & T_{\eta\eta}^{JL} & T_{\eta\pi^2}^{JL} \\ T_{\pi^2\pi}^{JL} & T_{\pi^2\eta}^{JL} & T_{\pi^2\pi^2}^{JL} \end{pmatrix}$$

where various channels are denoted by the index  $\pi$  for  $\pi N$ ,  $\eta$  for  $\eta N$  and  $\pi^2$  for all other channels ( $\pi\Delta$ ,  $\rho N$ ,  $\pi\pi N$ , ...). The third channel is effectively described as a two body process  $\pi^2 N$  with  $\pi^2$  being a quasiparticle with a different mass chosen for each partial wave. We have fixed the channel masses, for each partial wave independently.

## B. Single resonance model

The simplest possible model to represent the  $\pi N$  vertex, and which is directly comparable to earlier analyses [3,11,12,26], has been constructed. Only one resonance without any background terms is used to describe each of the three important partial waves  $S_{11}$ ,  $P_{11}$  and  $D_{13}$ .

The elastic T-matrix for each resonance is defined as:

$$T_{cc}^{JL}(W) = \frac{\Gamma_c^{JL}(W)/2}{M^{JL} - W - i\Gamma_{\text{tot}}^{JL}(W)/2}; \quad c = \pi, \eta, \pi^2. \quad (3)$$

The partial widths are given by:

$$\Gamma_c^{JL}(W) = \Gamma_c^{JL}(M^{JL}) \times \begin{cases} \left(\frac{q_c}{q_{0c}^{JL}}\right)^{2L+1} & \text{for } q_c < q_{0c}^{JL} \\ \left(\frac{2q_c}{q_c + q_{0c}^{JL}}\right)^{2L+1} & \text{for } q_c > q_{0c}^{JL} \end{cases} \quad (4)$$

and  $q_c$  is the c.m. momentum of the channel meson  $c$ :  $\pi$ ,  $\eta$ , or  $\pi^2$ :

$$q_c \equiv q_c(W) = \frac{\sqrt{(W^2 - (m + m_c)^2)(W^2 - (m - m_c)^2)}}{2W} \quad (5)$$

for  $m_c = m_\pi, m_\eta, m_{\pi^2}$ .  $q_{0c}^{JL} \equiv q_c(M^{JL})$  is the c.m. momentum of the channel meson  $c$  at the resonance mass  $M^{JL}$ .

The exception is  $P_{11}$  because its mass is below  $\eta$  threshold. For that case we use:

$$\Gamma_\eta^{P_{11}}(W) = \begin{cases} 0 & \text{below } \eta N \text{ threshold} \\ 100 \left(\frac{q_\eta}{410}\right)^3 & \text{above } \eta N \text{ threshold} \end{cases} \quad (6)$$

This definition of partial widths gives the correct threshold behavior for the T-matrix. The total widths are given as:

$$\Gamma_{\text{tot}}^{JL}(W) = \Gamma_\pi^{JL}(W) + \Gamma_\eta^{JL}(W) + \Gamma_{\pi^2}^{JL}(W). \quad (7)$$

The inelastic T-matrix is given by

$$T_{c_1 c_2}^{JL}(W) = \sqrt{T_{c_1}^{JL}(W) T_{c_1}^{JL}(W)} \quad c_1, c_2 = \pi, \eta, \pi^2, \quad (8)$$

and the T-matrix is defined in such a way as to give a unitary S matrix:

$$S = 1 + 2iT, \quad S^\dagger S = S S^\dagger = 1. \quad (9)$$

Reliable branching ratios of various resonances to the  $\eta$  channel unfortunately are not available except for  $S_{11}$ . As can be seen from Table 1, all values used in our calculation are within range of the accepted values [1]. However, the agreement of the elastic  $\pi N$  partial wave T-matrices values with the Karlsruhe - Helsinki phase shift analysis (K-H) [16] is not entirely satisfactory for the lower energy range  $T_\pi \leq 700$  MeV, and the single resonance model completely misses all higher energy partial waves in the elastic channels. The results are shown in Figs. 2a and 2b. The dashed-dotted line shows our single resonance model and the dotted line is the B-T single resonance model of Ref. [12] which has an additional energy dependent form factor. The B-T model is limited to lower energies. The dots are the elastic K-H  $\pi N$  partial wave analyses [16]. As the K-H PWA does not give the error analysis for the partial wave T-matrices in [16], and the errors are essential to define the statistical weight of the analyses, we have identified the errors of the used data in the standard  $\chi^2$  analysis as:

$$\Delta_i^{JL} = 0.005 + \left( 0.01 + 0.0015 \frac{W_i - W^{\pi \text{ thresh}}}{\Delta} \right) |T_{\text{max}}^{JL}|$$

$$\Delta = 1 \text{ GeV}$$

$W_i$  is the total c.m. energy

$W^{\pi \text{ thresh}}$  is the total energy at  $\pi$  nucleon threshold

$|T_{\text{max}}^{JL}|$  is the maximal value of the T – matrix in the chosen energy range.

The energy range extents up to 2.5 GeV of the total c.m. energy.

The statistical weight in the  $\chi^2$  function is defined in a standard way as well:

$$w_i^{JL} = \frac{1}{(\Delta_i^{JL})^2}.$$

The introduced energy dependence of the statistical weight is inspired by the energy dependence of the error analysis of Ref. [15]. It steadily raises with energy, but does not exceed the value of 0.02 in the units of Ref. [16].

The total cross sections for the  $\eta$  production are compared with the single resonance model (dash-dotted line) of this article, and the B-T single resonance model of Ref. [12] (dotted line) in Figs. 1a and 1b. The experimental data for the  $\eta$  production differential cross sections are compared with both models in Figs. 3a-3d. The full and dashed lines in Figs. 1-3 will be explained later.

The failure of single resonance model to describe the experimental facts is not unexpected. Even at the lower energies, background terms which are not included in the single resonance model are of some importance, and their omission can account for the observed discrepancy with the input. The comparison of the parameter free single resonance model, of this article (dash-dotted line), with the similar B-T model [12] (dotted line) shows a fair likeness in the energy range where the later analysis has been given. The differences between the two models are attributed to the different input data base and to the additional energy dependent form factor used in [12]. However, as is seen in Figs. 1-3, both models show reasonable agreement with the input data for the important  $\pi N$  elastic partial waves  $S_{11}$ ,  $P_{11}$  and  $D_{13}$  at lower energies. Our analysis predicts strong deviations from the fitted  $\pi N$  elastic partial waves at higher energies, for the  $S_{11}$  partial wave in particular, so it is to be expected that the results of [12] suffer from a similar disease for higher energies. Similar statements can be and are valid for the total and differential cross sections of  $\eta$  production (Figs. 1 and 3). The phenomenon observed is consistent with the fact that the single resonance model covers only the energy range of the first peak in  $\sigma_t(\pi p \rightarrow \eta n)$ .

Let us mention that in the described single resonance formalism it is not possible to extrapolate the model to include more than one resonance per partial wave in a straightforward manner without directly violating the S-matrix unitarity.

### C. A unitary multiresonance model

In order to fit the  $\pi N$  elastic amplitudes of Ref. [16] better than in single resonance model we have introduced a manifestly unitary model that enables including more than one resonance and background term per partial wave. It is constructed following the commonly accepted method developed in [15], and originally used in  $\pi N$  elastic partial wave analysis (PWA) [16]. \*

As the  $\eta$  meson is a pseudoscalar, isospin zero particle, it mixes by isospin violation with the  $\pi^0$ . We have chosen the following three coupled channels to set up

---

\*The simple recipe for the modification of the S-matrix, which consists in directly adding extra resonances and a smooth background is manifestly nonunitary.



the model: the  $\pi N$ ,  $\eta N$  and a third, an effective two body channel labeled  $\pi^2 N$ , which inclusively contains and represents all remaining, even three body channels ( $\pi\Delta$ ,  $\rho N$ ,  $\pi\pi N$ , etc.). The objective of the procedure is to simultaneously achieve a good representation of the input  $\pi N$  elastic T-matrices, and the experimental  $\eta$  production data (total and differential cross sections) by the values coming out of the model.

We distinguish three basic steps of the presented analysis.

### Step 1 - formalism

The multichannel  $T$  matrix taken over from [15] is given as:

$$T_{ab}^{JL} = \sum_{i,j=1}^{N^{JL}} f_a^{JL}(s) \sqrt{\rho_a} \gamma_{ai}^{JL} G_{ij}^{JL}(s) \gamma_{jb}^{JL} \sqrt{\rho_b} f_b^{JL}(s) \quad (10)$$

$a, b = \pi, \eta, \pi^2$ . The initial and final channels couple through intermediate "particles" or resonances labeled with  $i$  and  $j$ , and

$$f_a^{JL}(s) = \left( \frac{q_a}{Q_{1a} + \sqrt{Q_{2a}^2 + q_a^2}} \right)^L \quad (11)$$

$$\rho_a(s) = \frac{q_a}{\sqrt{s}} \quad (12)$$

where  $s = W^2$  and  $q_a$  is the meson momentum for any of the three channels given as:

$$q_a \equiv q_a(W) = \frac{\sqrt{(W^2 - (m + m_a)^2)(W^2 - (m - m_a)^2)}}{2W}. \quad (13)$$

The mass parameter  $m_{\pi^2}$  for the  $\pi^2 N$  channel is fixed prior to minimization to the mass value at which the partial wave inelasticities show the opening of the first inelastic channel:

Partial wave	S <sub>11</sub>	P <sub>11</sub>	P <sub>13</sub>	D <sub>13</sub>	D <sub>15</sub>	F <sub>15</sub>	F <sub>17</sub>	G <sub>17</sub>
$m_{\pi^2}$ (MeV)	450	380	370	380	400	370	650	450

$\gamma_{ia}^{JL}$  are free parameters and will be determined by the fitting procedure. For the  $Q_{1a}$  and  $Q_{2a}$  parameters we choose the values

$$\begin{aligned} Q_{1\pi} &= Q_{2\pi} = m_\pi \\ Q_{1\eta} &= Q_{2\eta} = m_\eta \\ Q_{1\pi^2} &= Q_{2\pi^2} = 400 \text{ MeV} \end{aligned} \quad (14)$$

$G_{ij}^{JL}$  is a dressed propagator for partial wave  $JL$  and particles  $i$  and  $j$ ;

$$G_{ij}^{JL}(s) = G_{ij}^{0JL}(s) + \sum_{k,l=1}^{N^{JL}} G_{ik}^{0JL}(s) \Sigma_{kl}^{JL}(s) G_{lj}^{JL}(s). \quad (15)$$

The bare propagator

$$G_{ij}^{0JL}(s) = \frac{e_i \delta_{ij}}{s_i - s} \quad (16)$$

has a pole at the real value  $s_i$ . The sign  $e_i = \pm 1$  must be chosen to be positive for poles above the elastic threshold which correspond to resonances. The nonresonant background is described by a function that consists of two terms of the form (16) with pole positions below  $\pi N$  threshold. For that case signs of terms are opposite. The positive sign correspond to the repulsive and negative to the attractive potential.  $\Sigma_{kl}^{JL}$  is the self-energy term for the particle propagator:

$$\Sigma_{kl}^{JL}(s) = \sum_a \gamma_{ka}^{JL} \Phi_a^{JL}(s) \gamma_{la}^{JL} \quad (17)$$

The imaginary part of  $\Phi_a^{JL}(s)$  is the effective phase-space factor for the channel  $a$ :

$$Im \Phi_a^{JL}(s) = [f_a^{JL}(s)]^2 \rho_a(s) \equiv F_a^{JL}(s) \quad (18)$$

The real part of  $\Phi_a^{JL}(s)$  is calculated using a subtracted dispersion relation

$$\Phi_a^{JL}(s) = \frac{s - s_0}{\pi} \int_{s_a}^{\infty} \frac{F_a^{JL}(s')}{(s' - s)(s' - s_0)} ds' \quad (19)$$

where  $s_a = (m + m_a)^2$ .

The advantage of this approach is that it manifestly maintains the  $S$  matrix unitarity for any number of resonance and/or background terms. The disadvantage is that the connection of the parameters  $\gamma_{ia}^{JL}$  and  $s_i$  with the conventional resonance parameters  $M_i^{JL}$  and  $\Gamma_{ia}^{JL}$  is not direct [15], but has to be calculated.

## Step 2 - data base and fitting procedure

The input parameters for the fitting procedure are  $s_i$  and  $\gamma_{ia}$  which determine the bare propagator and self energy term for the particle propagator, see Eqs. (14),(15) and (16) respectively. The parameters  $Q_{1a}$  and  $Q_{2a}$  which occur in the form factor given in Eq. (10) have been fixed to the mass of the channel  $a$  meson. The ones subtracted dispersion relation given in Eq. (19) is solved numerically with the

subtraction constant  $s_0 = s_a$  and  $\Phi_a^{JL}(s_0) = 0$ . The stability of the solution has been tested by calculating and reproducing the initial imaginary part, see Eq.(18). The numerical integration has been performed using the adapted Gaussian quadrature method with no significant dependence on the number of points. We should mention that the dispersion relation has been calculated only once, and tabulated for further use to save the CPU because the parameters which form the integrand are not varied in the minimization procedure.

### Data base

As the input data to the minimization procedure we have used:

1. the K-H partial wave  $\pi N$  analyses [16]
2. total cross sections for the  $\pi N \rightarrow \eta N$  process [13,17–23,28]
3. differential cross sections for the  $\pi N \rightarrow \eta N$  process [13,17–20,22,23,28]

We have fitted the  $\pi N$  elastic  $T$  matrices for eight  $I = 1/2$  partial waves:  $S_{11}$ ,  $P_{11}$ ,  $P_{13}$ ,  $D_{13}$ ,  $D_{15}$ ,  $F_{15}$ ,  $F_{17}$  and  $G_{17}$  using the phase shift analysis K-H [16] at 90 energies from threshold to 2.5 GeV of the total c.m. energy. We have also tested the use of (CMU-LBL)  $\pi N$  elastic partial wave analyses [15] without any notable differences. At the inception of this work the only PWA that covered the high energy was K-H [16]. Since then the VPI group [27] has extended its analysis approximately to 2.1 GeV. We do not anticipate that the use of VPI PWA would introduce any substantial changes into the conclusions coming out of the present analysis. Anyhow, a new analysis based on the VPI PWA is planned to be the subject of a future research. Finally, let us comment that we should have used the total set of experimental data for  $\pi N$  elastic processes instead of limiting the input to the model dependent information coming from PWAs. However, we have assumed that existing PWAs represent the data adequately enough so we can avoid an enormous CPU time consumption.

The data for the second,  $\eta N$  channel, are the  $\pi N \rightarrow \eta N$  differential cross sections at 81 energies and total  $\eta N$  production cross sections at 67 energies [13,17–23,28]. The statistical weights of for the  $\eta N$  data, used in the minimization procedure, have been based on the analysis of the world data give in Ref. [14]. In some cases the published statistical weight had to be modified. Problems of consistency among different measurements have been extensively discussed in [14], and the discrepancy

for the lower energies of  $\eta$  production differential cross section of data of Ref. [13] has been claimed. It has been argued in Ref. [14] the data of Ref. [13] are systematically too low, and that it is due to an error in the beam momentum calibration which makes the data at lower energies essentially unusable even if one tries to correct them by a momentum shift. The direct reason for that is a strong momentum dependence of the lab  $\Leftrightarrow$  c.m. transformation Jacobian. However, at higher energies, it is safe just to perform a 4 % momentum shift downward. Therefore, the systematic error, in addition to the published, statistical one, has been added to the questionable data sets reducing their statistical impact. The statistical weight of all differential cross sections of Ref. [13] has been reduced by the factor of 2. In addition, the statistical weight at lowest energies of  $W = 1511$  MeV,  $1542$  MeV and  $1571$  MeV has been even more reduced so that their importance in the analysis is practically eliminated.

A systematic error of  $0.01$  mb/sr has been added to *all*  $\eta$  production differential cross sections. We have decided to do so because of the fact that the quoted errors in all measurements have been of statistical origin only, so most of the errors have been unrealistically low.

The data taken at the energy of  $1507$  MeV in Ref. [19] as well tend to be too low when the total cross section is calculated [14] and compared to the "world trend". Therefore, the additional systematic error of  $0.04$  mb/sr have been added to these data.

For similar general reasons the systematic error of  $0.02$  mb/sr has been added to all the data of Ref. [28].

All "two star" cross sections, as given in Ref. [14] are taken with the increased statistical factor of 10, while the statistical factor of the remaining cross section data is kept to be 1.

The direct consequence of our choice of the data base statistical weights is seen in Fig. 3a: Ref. [12] reproduces the data set of Ref. [13] at lower energies ( $W = 1511, 1546$  and  $1571$  MeV) while our result tends to reproduce other sets much better. Additional, precise measurements for that process are needed in order to eliminate the present uncertainties.

### **Fitting procedure**

We have fitted the 8 above listed lowest  $I = 1/2$  partial waves in the following manner:

- a. The number of resonances and the shape of the background is determined by the choice of bare propagator and self energy term parameters. We have decided to start from the number of resonances in each partial wave as given in [1,16]; the background is represented by two resonant functions with the constraint that the pole position is far outside the physical region. Only one resonance in the  $P_{13}$  and  $F_{15}$  partial waves has been used in our analysis, higher (uncertain) resonances have been dropped. The existence of the second  $P_{13}$  resonance has been recently suggested, and it was used in the M-S  $\pi N$  analyses [24,25].
- b. In general, we need up to two background terms. They have been numerically represented as tails of resonances having their pole positions far outside the analyzed energy range\*.
- c. Error analysis for resonance parameters has been done on the basis of MINUIT, imposing the confidence level of 70 % [29].

We have used a standard MINUIT program using as much as 132 parameters in the final run.

The minimization has been complicated, and a lot of technical tricks had to be used to avoid occurrence of local minima which are hard to handle for a minimization with such a number of parameters.

The result of the fitting procedure gives us a full three channel T-matrix, with submatrices describing the  $\pi N \rightarrow \eta N$  and  $\eta N \rightarrow \eta N$  processes.

### **Step 3 - resonance parameters**

The pole positions, resonance masses and widths have to be obtained numerically from the full partial wave T-matrix, following directly the technique developed in [15]. For the convenience of the reader we shall briefly reproduce the essential steps, angular momentum indexes are suppressed.

The poles of T-matrix given in Eq.(10) are found solving the following equation:

$$\det G^{-1} = 0. \tag{20}$$

The eigenvector of the matrix  $H \equiv G^{-1}$  has been found at the pole position  $s_{\text{pole}}$ :

---

\*More than one background term was needed in order to obtain some nontrivial, but smooth energy dependent behavior of the background terms.

$$\sum_j H_{ij}(s_{\text{pole}})\chi_j = 0. \quad (21)$$

We have defined quantities:

$$\eta_c = \sum_i \gamma_{ic}\chi_i \quad (22)$$

which define the coupling of resonance  $i$  to the channel  $c$ . We consider the width to be an energy-dependent quantity involving the phase-space factors:

$$\begin{aligned} \Gamma &\sim \sum_c y_c F_c(s) \\ y_c &= |\eta_c|^2. \end{aligned} \quad (23)$$

Near the resonance we parametrize the T-matrix as:

$$T_{ab} = (B_{ab} - \delta_{ab})/2i + \sum_{cd} B_{ac}^{1/2} F_c^{1/2} \eta_c D^{-1} \eta_d F_d^{1/2} B_{db}^{1/2} \quad (24)$$

where  $B_{ab}$  is a background S-matrix and the generalized Breit-Wigner denominator is:

$$D(s) = r - s - c \sum_c y_c \Phi_c(s). \quad (25)$$

The real constants  $r$  and  $c$  are chosen so that  $D(s_{\text{pole}}) = 0$ . The resonance mass, width and the branching ratios are defined as:

$$\begin{aligned} \text{Re } D(M^2) &= 0 \\ \Gamma &= \frac{\text{Im } D(M^2)}{M \text{Re } D'(M^2)} \\ \Gamma_c &= \frac{y_c F_c(M^2) \Gamma}{\sum_a y_a F_a(M^2)} \equiv x_c \Gamma \end{aligned} \quad (26)$$

where  $D'$  is the derivative of the generalized Breit-Wigner denominator (25). The obtained resonance parameter values are given in Tables 2 and 3.

### III. RESULTS OF THE UNITARY MULTIRESONANCE MODEL WITH THREE $P_{11}$ RESONANCES

We have obtained the partial wave T-matrices for  $\pi N$  elastic scattering (see Figs. 2a and 2b),  $\pi N \rightarrow \eta N$  (see Figs. 4a and 4b) and  $\eta N$  elastic scattering (see

Figs. 5a and 5b), on the basis of our fit to the  $\pi N$  elastic and  $\pi N \rightarrow \eta N$  data. The agreement with the input  $\pi N$  elastic K-H PWA T-matrices is given in Fig. 2, while the agreement with the input  $\pi N \rightarrow \eta N$  differential cross sections is given in Fig. 3. The full, dash-dotted and dotted lines systematically denote the results of our multiresonance, and the two single resonance models, this publication and B-T respectively. The T-matrix for  $\eta N$  elastic scattering is a prediction. All observables, obtainable on the basis of our results for the partial wave T-matrix of the  $\pi N \rightarrow \eta N$  and  $\eta N$  elastic reactions, with the exception of the  $\pi N \rightarrow \eta N$  differential cross sections, which are input data, are henceforth a prediction. Our T matrices can be used as input to  $\eta$  production calculations in reactions such as  $pp \rightarrow pp\eta$ .

As can be seen, single resonance models give a reasonable agreement only in the region of the  $S_{11}(1535)$ . They can be used for higher order calculations only, for a limited energy range where one resonance per partial wave dominates. However, the analyses presented in this article, which is based on more than one resonance per partial wave, can be used over the full energy range.

The results of the multiresonance model for the  $\pi N$  interaction by M-S [24] can be used as a consistency check. The parameters of both models, for the same number of resonances per partial wave ( those given by the PDG [1]) are listed in Table 2. We may call these analyses complementary because the inelastic part of the  $\pi N$  partial waves is constrained by two complementary processes:  $\eta$  production in our case, and continuum production in the case of Ref. [24]. Therefore, the  $\pi^2$  part of our analysis should roughly correspond to the  $\pi\pi$  part of another analyses, and the parameters of the  $\eta$  production partial waves explicitly included in other analyses should correspond to our findings. Of course, masses and widths of resonances should correspond to the values given by the K-H and CMU-LBL  $\pi N$  elastic analyses, which are generally accepted by PDG [1].

As can be seen from our Figs. 1-3, the multiresonance model, based on the standard number of resonances describes the input  $\pi N \rightarrow \pi N$  and  $\pi N \rightarrow \eta N$  data fairly well. Of course, the  $\eta$  production cross sections are as well correctly described in the full energy range. The structure of the  $\pi N$  elastic partial waves [16] is not entirely reproduced. The tendency of smoothing elastic partial waves, as it has been already indicated previously, exists when the inelastic channels are explicitly included. Therefore, we are tempted to conclude that inclusion of inelastic processes imposes some restrictions on the elastic channel forcing partial waves to have less

structure then in [16].

Comparing the available analyses we conclude:

1. The masses and  $\pi N$  elastic branching ratios generally agree for all three PWA, with the exception of the  $P_{11}$ . This problem is discussed later.
2. All partial waves *except* the  $P_{11}$  show reasonable agreement in both multichannel models.
3. The two higher  $P_{11}$  partial wave resonances of M-S and our analyses do not agree. The branching ratio for  $\eta$  production in our model is about 90 %. The M-S model [24] predicts almost a 60 % branching ratio to the  $\pi\pi$  channel, leaving no freedom for any flux going to the  $\eta$  production channel. The disagreement is obvious, and we shall offer a natural explanation.

#### IV. RESULTS OF THE UNITARY MULTIRESONANCE MODEL WITH FOUR $P_{11}$ RESONANCES

Inspection of the resonance parameters of Ref. [24] reveals the following (see Table 2.):

- the total width of the  $P_{11}(\overset{51}{1440/135})$  is different from the ones of K-H [16], CMU-LBL [15] and Arndt et al. [27]
- the total width of the  $P_{11}(\overset{12}{1710/120})$  is different from the ones of K-H [16], CMU-LBL [15] and Arndt et al. [27]
- the mass the  $P_{11}(\overset{9}{2100/200})$  is much lower than the ones of K-H [16] and CMU-LBL [15]
- the mass of the  $D_{13}(\overset{6}{2080/265})$  is shifted from 2080 to 1804 MeV

Therefore, we suspect that a part of the physics in the vicinity of the 1800 MeV mass region is not entirely taken into account.

*We assume that there is another degree of freedom in the  $P_{11}$  partial wave, in the form of another resonance.*



This possibility of having four instead of three resonances in the  $P_{11}$  channel leads to a fit which is shown in the figures with dashed lines. The resonance parameters are given in Table 3. The T-matrix pole positions for K-H [16], CMU-LBL [15], M-S [24] and our analyses (3 and 4 poles) are given in Fig. 6\*. As can be seen in Fig. 6, the pole positions of the three resonances are well established in the classical  $\pi N$  elastic PWAs and are fairly close. The  $P_{11}$  T-matrix pole positions for the M-S analysis [24] (given by filled circles) are quite different from the recommended values. The three pole version of the  $P_{11}$  of our calculation is also quite compatible with the K-H and CMU-LBL pole positions. The four pole version of the  $P_{11}$  shows agreement for the lowest pole, the next two poles are near in masses, but distinctly separated in the complex energy plane, while the fourth pole is somewhat lower than K-H. In our analysis the fourth resonance is strongly inelastic, going mainly to the  $\eta$  production channel, therefore it is not to be expected that either of the K-H or M-S analyses could determine it with great precision.

## V. CONCLUSIONS

1. The addition of another resonance in the  $P_{11}$  partial wave definitely improves our fit to elastic and inelastic data in all channels. Various quark models also predict four and even five  $P_{11}$  resonances in the energy region of 1440 to 2200 MeV [30,31].
2. The changes in  $\pi N$  elastic partial waves are negligible because all the resonances (with the exception of the first one) are strongly inelastic.
3. The changes in  $\eta$  production and  $\eta N$  elastic channel T-matrices are clearly visible in all partial waves. As it is to be expected, the  $P_{11}$  is significantly changed, while other partial waves do show some variation. However, let us draw the readers attention to the fact that  $S_{11}$ ,  $P_{11}$  and  $D_{13}$  partial waves are the dominant ones, while the contribution of other channels is at least the order of magnitude lower. So, even if the relative change in Figs. 4 and 5. is

---

\*CMU-LBL and our analyses give the exact T-matrix pole positions, while the poles for the remaining analyses have been approximated by  $M - i\Gamma/2$ .

large for other partial waves, the change at the absolute scale is comparably small.

4. The inconsistency problem between the two inelastic PWAs goes away. The two  $P_{11}$  resonances in the vicinity of 1750 MeV are responsible for the continuum production, this is to be compared with 1717 and 1885 resonances of Ref. [24], the third resonance at 2215 almost completely couples to the  $\eta N$  channel, with a very small branching ratio to the continuum production.
5. The M-S PWA [24] could not easily see the additional fourth  $P_{11}$  resonance as it mostly couples to the  $\eta$  production channel, and it is not, in their case, explicitly included.
6. The elastic  $\pi N$  analyses [16,15] have problems of determining the number and parameters of the resonances going to inelastic channels. Some changes in the resonances with a small elastic branching ratio should be easy to obtain in the single channel formalism.
7. If the Brown data for  $T_\pi > 900$  MeV are shifted to lower energies by 30 MeV and data below 900 MeV are omitted then the resonance parameters for our solutions containing 3 and 4 resonance in the  $P_{11}$  are shown in Table 4. The results are virtually identical (within errors) with the solutions using all originally published Brown data [13]. That indicates that our PWA is showing robustness with respect to possible errors in input.

Of course, adding extra  $P_{11}$  resonance is only one way of making our analysis compatible to M-S PWA, there might be other, equally good explanations of the apparent disagreements when the inelastic branching ratios are compared. One technical detail has to be kept in mind: the background parts are represented by two resonances with poles kept far outside the range of interest. Therefore, the background is also fitted. The proper way should be to calculate the background in some model (for instance a cloudy bag model), to fix it, and then fit just the resonant part [32]. The interference of background and resonant parts might shift the resonance parameters notably.

The T matrices obtained in this study are an essential ingredient for calculating  $\eta$  production reactions  $D(\pi, NN)\eta$  and  $D(\pi, NN)\pi$ . The off mass shell extrapolation

procedure for the  $\eta$  production amplitudes can not be determined in this formalism. We do hope to learn something about these effects from the higher order processes, assuming that the off-mass shell behavior of the  $\eta$  particle is similar as of the pions [33]. \*

---

\*This work has been partly supported by the EC contract C11\*-CT-91-0894 and DOE contract DE - FG03 - 88ER40420/A606.

- 
- [1] Particle data group, Phys. Rev., **D45** (1992)
- [2] G. Höhler, in  $\pi N$  Newsletter, **No 9** ed: G. Höhler, V. Kluge, B.M.K.Nefkens, 1 (1993)
- [3] R.S. Bhalerao, L.C. Liu, Phys. Rev. Lett., **54**, 865 (1985)
- [4] M. Arima, K. Shimizu, K. Yazaki, Nucl. Phys., **A243**, 613 (1993)
- [5] C. Wilkin, Phys. Rev., **C 47**, 938 (1993)
- [6] L.C. Liu, Q. Haider, Phys. Rev., **C 34**, 1845 (1986)
- [7] B.Krusche, Proc. of the I TAPS Workshop, Alicante 1993 (World Scientific)
- [8] T. Vetter, A. Engel, T. Biro and U. Mosel Phys. Lett., **B263**, 153 (1991)
- [9] J.M. Laget, F. Wellers and J.F. Lecomte, Phys. Lett., **B257**, 254 (1991)
- [10] R.C. Carrasco, Phys. Rev., **C48**, 2333 (1993)
- [11] H.C. Chiang, E. Oset and L.C. Liu, Phys. Rev., **C44**, 738 (1991)
- [12] C. Bennhold and H. Tanabe, Nucl. Phys., **A350**, 625 (1991)
- [13] R.M. Brown, A.G. Clark, P.J. Duke, W.M. Evans, R.J. Gray, E.S. Groves, R.J. Ott, H.R. Renshall, A.J. Shah, J.J. Thresher and M.W. Tyrrell, Nucl. Phys., **B153**, 89 (1979)
- [14] M. Clajus and B.M.K. Nefkens, in  $\pi N$  Newsletter, **No 7**, ed. G. Höhler, W. Kluge and B.M.K. Nefkens, 76 (1992)

- [15] R.E. Cutkosky, R.E. Hendrick, J.W. Alcock, Y.A. Chao, R.G. Lipes, J.C. Sandusky and R.L. Kelly, Phys. Rev., **D20**, 2804 (1979), R.E. Cutkosky, C.P. Forsyth, R.E. Hendrick and R.L. Kelly, Phys. Rev., **D20**, 2839 (1979), R.K. Kelly and R.E. Cutkosky, Phys. Rev., **D 20** 2782 (1979),
- [16] G. Höhler, *in* Landolt-Börnstein, Elastic and Charge Exchange Scattering of Elementary Particles, Vol. **9**, Subvolume **b**: Pion Nucleon Scattering, **Part 2** (1983)
- [17] W. Deinet, H. Müller, D. Schmitt, H.M. Staudenmaier, S. Buniatov and E. Zavattini, Nucl. Phys., **B11**, 495 (1969)
- [18] F. Bulos, R.E. Lanou, A.E. Pifer, A.M. Shapiro, C.A. Bordner, A.E. Brenner, M.E. Law, E.E. Ronat, F.D. Rudnick, K. Strauch, J.J. Szymanski, P. Bastien, B.B. Brabson, Y. Eisenberg, B.T. Feld, V.K. Kistiakowsky, I.A. Pless, L. Rosenson, R.K. Yakamoto, G. Calvelli, F. Gasparini, L. Guriero, G.A. Salandin, A. Tomasin, L. Ventura, C. Voci and F. Waldner, Phys. Rev., **187**, 1827 (1969)
- [19] B.W. Richards, C.B. Chiu, R.D. Eandi, C.A. Helmholtz, R.W. Kenney, B.J. Moyer, J.A. Poirier, R.J. Cence, V.Z. Peterson, N.K. Sehgal and V.J. Stenger Phys. Rev., **D1**, 10 (1970)
- [20] J.E. Nelson, thesis LBL, **1019** (1972)
- [21] D.M. Binnie et al, Phys. Rev., **D8**, 2793 (1973)
- [22] J. Feltesse, R. Ayed, P. Bareyre, P. Borgeaud, M. David, J. Erwein, Y. Lemoigne and G. Villet, Nucl. Phys., **B93**, 242 (1975)
- [23] R.B. Chaffee, thesis LBL, **1060** (1975)

- [24] D.M. Manley and E.M. Saleski, Phys. Rev. D, **45**, 4002 (1992) and references therein
- [25] D.M. Manley,  $\pi N$  Newsletter, **8**, 141 (1993)  
 Proceedings of the 5<sup>th</sup> International Symposium on Meson - Nucleon Physics and the  
 Structure of the Nucleon, Volume I, Boulder, Colorado, September 6 - 10, 1993
- [26] Q. Haider and L.C. Liu, Phys. Lett., **B172**, 257 (1986)
- [27] R.A. Arndt, Li Zhujun, L.D. Roper, R.L. Workman, J.M. Ford, Phys. Rev., **D 43**,  
 2131 (1991)
- [28] N.C. Debenham, D.M. Binnie, L. Camilleri, J. Carr, A. Duane, D.A. Garbutt, W.G.  
 Jones, J. Keyne, I. Siotis and J.G. McEwen, Phys. Rev., **D12**, 2545 (1975)
- [29] MINUIT Reference Manual, Ver. 92.1, Application Software Group, CERN Program  
 Library Long Writeup **D506**, 75 (1992)
- [30] R. Koniuk and N. Isgur, Phys. Rev., **D 21**, 1868 (1980)
- [31] S. Capstik and W. Roberts, Phys. Rev., **D 49**, 4570 (1994)
- [32] T.-S.H. Lee, private communication
- [33] M. Batinić, T.-S.H. Lee, M.P. Locher, Y. Lu and A. Švarc, *presented at Few Body  
 XIV*, Williamsburg (May-June 1994)

## TABLE CAPTIONS

**Table 1.** *Resonance parameters of the single resonance model.*

**Table 2.** *Resonance parameters of the multiresonance model with 3  $P_{11}$  resonances.*  
 The results of elastic  $\pi N$  analyses [1,16,15] are given in the first column. The

results of the partial wave analysis of this article, as well as results of the PWA of Ref. [24] are given in columns 2-10.

**Table 3.** *Resonance parameters of the multiresonance model with 4  $P_{11}$  resonances.*

**Table 4.** *Resonance parameters of the multiresonance models with 3  $P_{11}$  and 4  $P_{11}$  resonances using the data of Ref. [13], for  $T_\pi > 900$  MeV shifted downward by 30 MeV. Brown data below 900 MeV are omitted from fitting procedure.*

### FIGURE CAPTIONS

**Fig. 1.** The total  $\eta$  production cross sections. The experimental data are taken from the literature, as it has been indicated in the figure itself. The dotted line is the approximation that only one resonance has a strong branching ratio to the  $\eta$  production channel, the results are taken from [12]. The dash-dotted line is the result of this calculation, and is based on similar assumptions. The full line is the result of the three coupled channel multiresonance model presented in this publication with the number of resonances given by the PDG [1], namely three in the  $P_{11}$  partial wave. The dashed line is the four  $P_{11}$  resonance model. The full lines and the dashed lines show notable difference for the energies above  $T_\pi \geq 800$  MeV. The four resonance model for  $P_{11}$  is closer to experimental data.

Fig. 1a is the entire energy range available.

Fig. 1b is the same data, with an expanded scale for  $T_\pi$  up to 800 MeV.

**Fig. 2.** The  $\pi N$  elastic partial waves. The filled circles are the result of the single channel  $\pi N$  elastic PWA given in Ref. [16]. The used PWA does not give the error analyses for the partial wave T-matrices in [16], so the error bars given in the figure are defined in the text and reflect the statistical weight of the data set used in the minimization procedure. The dotted line is the approximation that only one resonance has a strong branching ratio to the  $\eta$  production channel, the results are from [12]. The dash-dotted line is the result of this calculation, and is based on similar assumptions. The full line is the result of the three coupled channel multiresonance model presented here

with the number of resonances given by the PDG [1], namely three in  $P_{11}$  partial wave. The dashed line is the four  $P_{11}$  resonance model. The full and the dashed lines are practically indistinguishable for all elastic partial waves.

**Fig. 3.** The comparison of the  $\eta$  production differential cross sections with the afore mentioned PWAs. The experimental data taken from the literature are defined in the figure. Curves are as in Fig. 2.

**Fig. 4.** The partial wave T matrix for the  $\eta$  production channel. The dash-dotted line is the single resonance approximation for  $S_{11}$ ,  $P_{11}$  and  $D_{13}$  partial waves of this article. The full line is the result of the three coupled channel multiresonance model presented here, with the number of resonances given by the PDG [1], namely three in  $P_{11}$  partial wave. The long dashed line represents the increase to four resonances in the  $P_{11}$  partial wave. Differences between long dashed and full lines are quite notable in this figure.

**Fig. 5.** The partial wave T matrix for the  $\eta N$  elastic channel. Differences between dashed (4  $P_{11}$  resonances) and full lines (3  $P_{11}$  resonances) are quite pronounced.

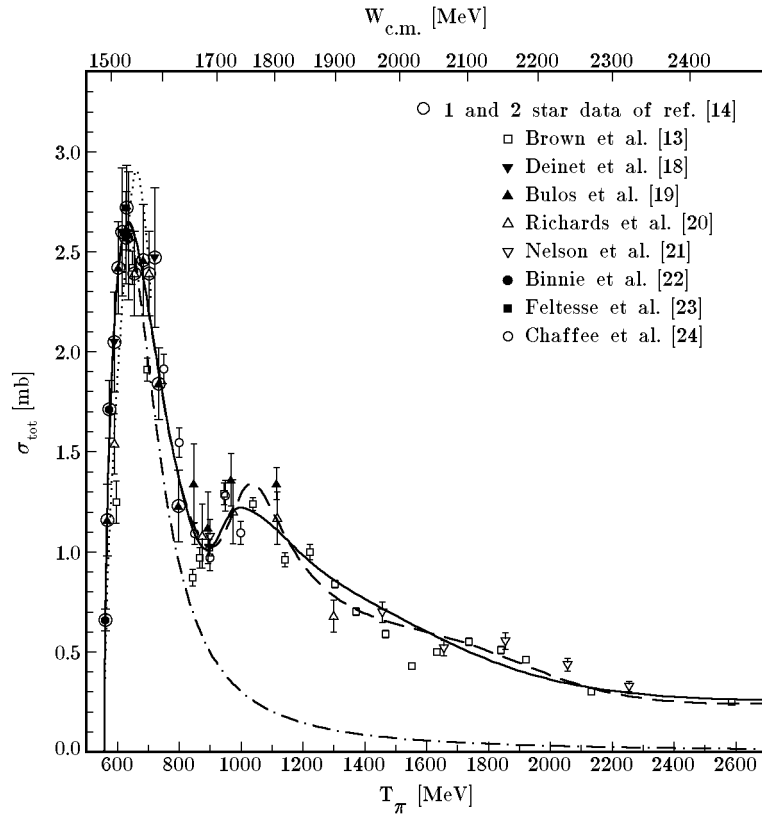
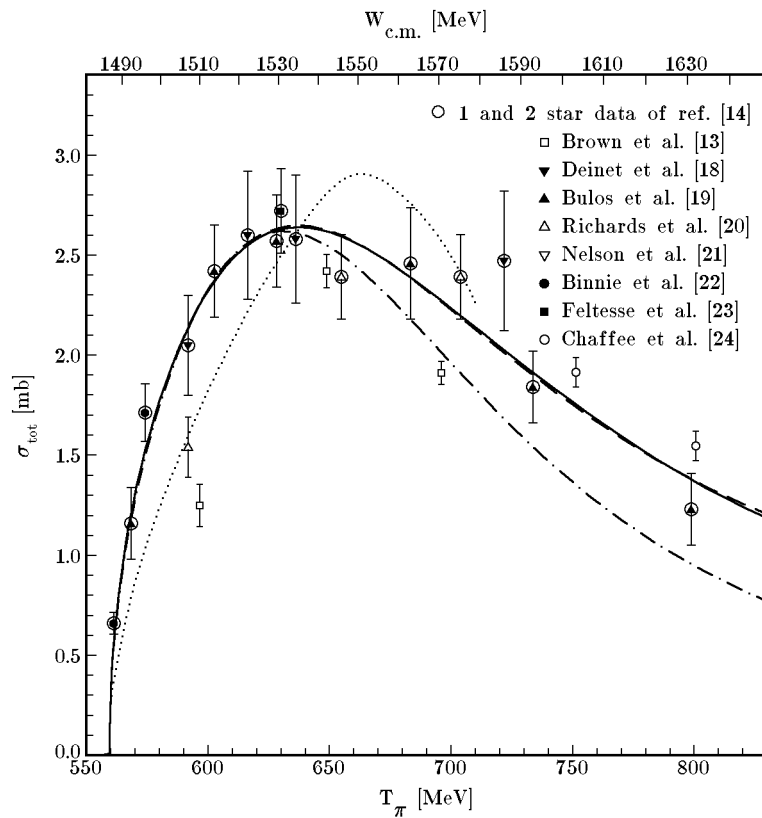
**Fig. 6.** The pole positions for all four partial wave analyses, mentioned in this article. The notation is given explicitly in the figure.



**Table 1**

Resonance	P.D.G parameters	Used parameters
S11(1535)	m = 1520 to 1555	1535
	$\Gamma = 100$ to 250	150
	$x_\pi = 0.35$ to 0.55	0.40
	$x_\eta = 0.30$ to 0.50	0.42
P11(1440)	m = 1430 to 1470	1440
	$\Gamma = 250$ to 450	250
	$x_\pi = 0.60$ to 0.70	0.60
	$x_\eta = 0$	0 <sup>*)</sup>
D13(1520)	m = 1515 to 1530	1520
	$\Gamma = 110$ to 135	120
	$x_\pi = 0.50$ to 0.60	0.55
	$x_\eta \sim 0.001$	0.0015

<sup>\*)</sup> $x_\eta = 0$  i.e.  $\Gamma_\eta = 0$  is used below,  $\Gamma_\eta = 100(\frac{q_\eta}{410})^3$  above  $\eta N$  threshold (see text).

**Fig. 1****(a)****(b)**

$\pi^- p \rightarrow \eta n$  total cross section:

( $\cdots$ ) Bennhold Tanabe,

(- · - ·) single resonance model,

(—) multiresonance unitary model with 3 resonances in P11,

(- -) multiresonance unitary model with 4 resonances in P11.

This figure "fig2-1.png" is available in "png" format from:

<http://arxiv.org/ps/nucl-th/9501011v2>

This figure "fig3-1.png" is available in "png" format from:

<http://arxiv.org/ps/nucl-th/9501011v2>

This figure "fig4-1.png" is available in "png" format from:

<http://arxiv.org/ps/nucl-th/9501011v2>

This figure "fig5-1.png" is available in "png" format from:

<http://arxiv.org/ps/nucl-th/9501011v2>

This figure "fig6-1.png" is available in "png" format from:

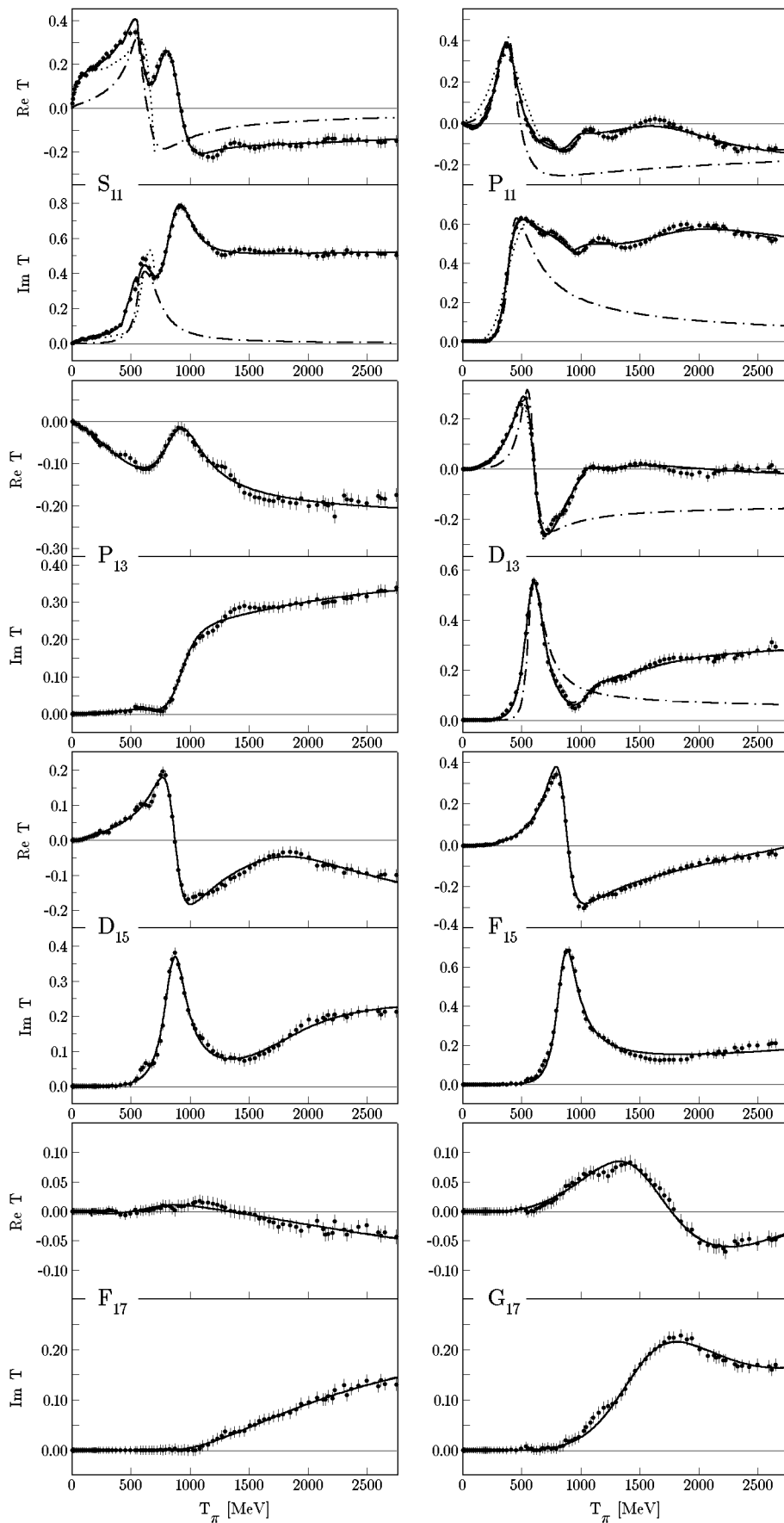
<http://arxiv.org/ps/nucl-th/9501011v2>

This figure "fig2-2.png" is available in "png" format from:

<http://arxiv.org/ps/nucl-th/9501011v2>



Fig. 2



$\pi N$  elastic T matrix :  
 (●) KH PWA,  
 (.....) Benhold & Tanabe,  
 (- · - ·) single resonance model,  
 (—) multiresonance unitary model with 3 resonances in P11,  
 (— —) multiresonance unitary model with 4 resonances in P11.

This figure "fig3-2.png" is available in "png" format from:

<http://arxiv.org/ps/nucl-th/9501011v2>

This figure "fig4-2.png" is available in "png" format from:

<http://arxiv.org/ps/nucl-th/9501011v2>

This figure "fig5-2.png" is available in "png" format from:

<http://arxiv.org/ps/nucl-th/9501011v2>

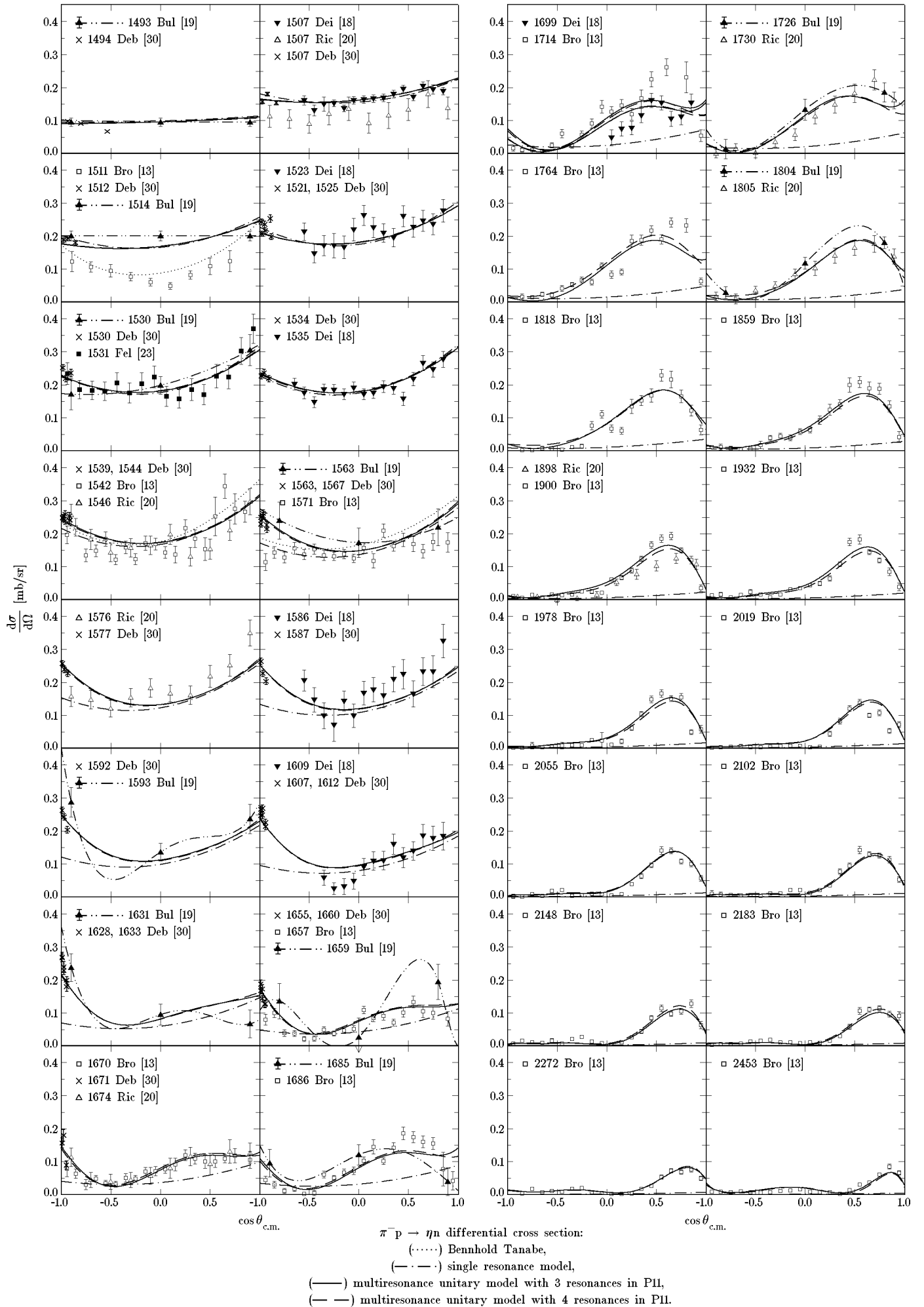
This figure "fig2-3.png" is available in "png" format from:

<http://arxiv.org/ps/nucl-th/9501011v2>

This figure "fig3-3.png" is available in "png" format from:

<http://arxiv.org/ps/nucl-th/9501011v2>

Fig. 3



This figure "fig4-3.png" is available in "png" format from:

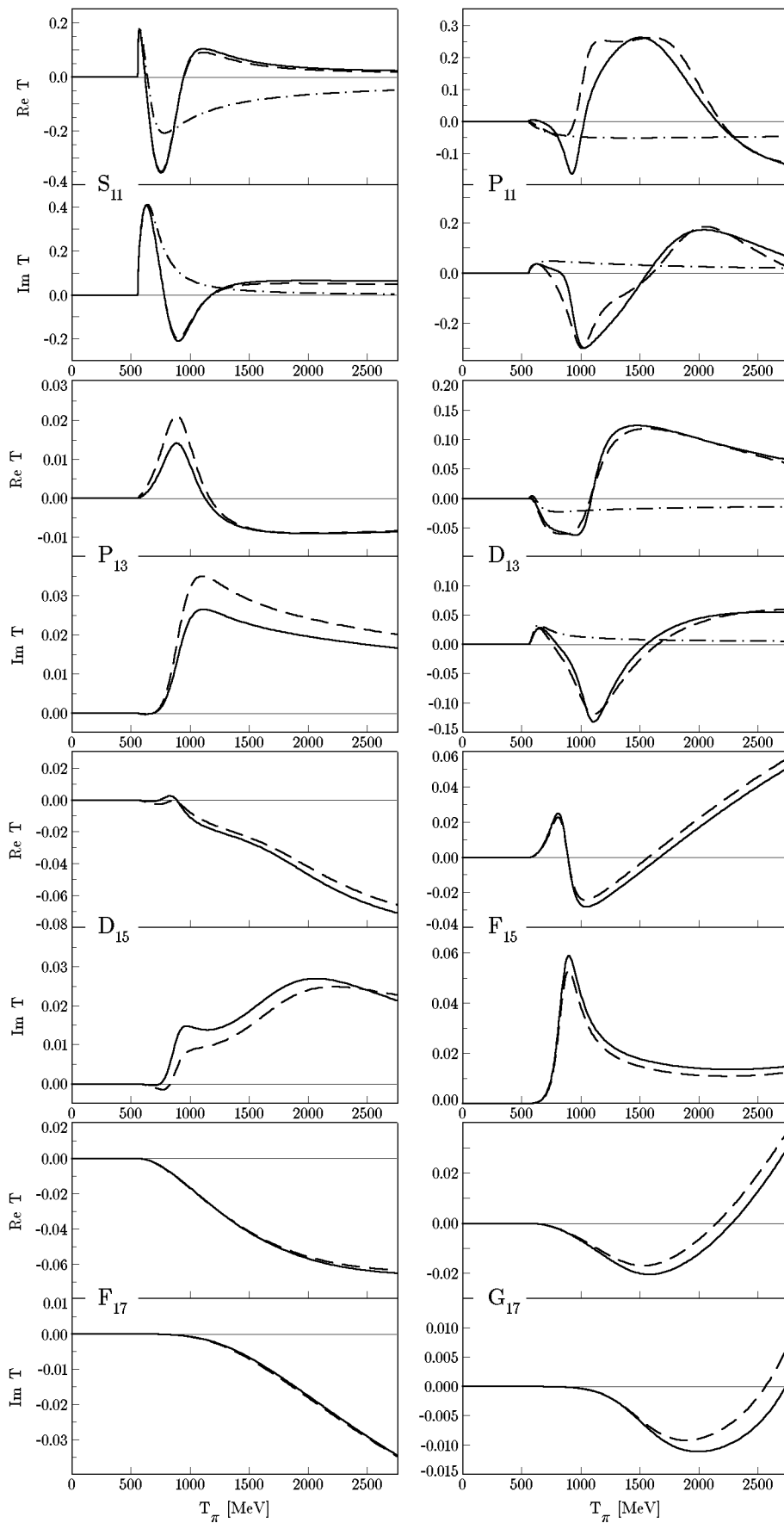
<http://arxiv.org/ps/nucl-th/9501011v2>



This figure "fig5-3.png" is available in "png" format from:

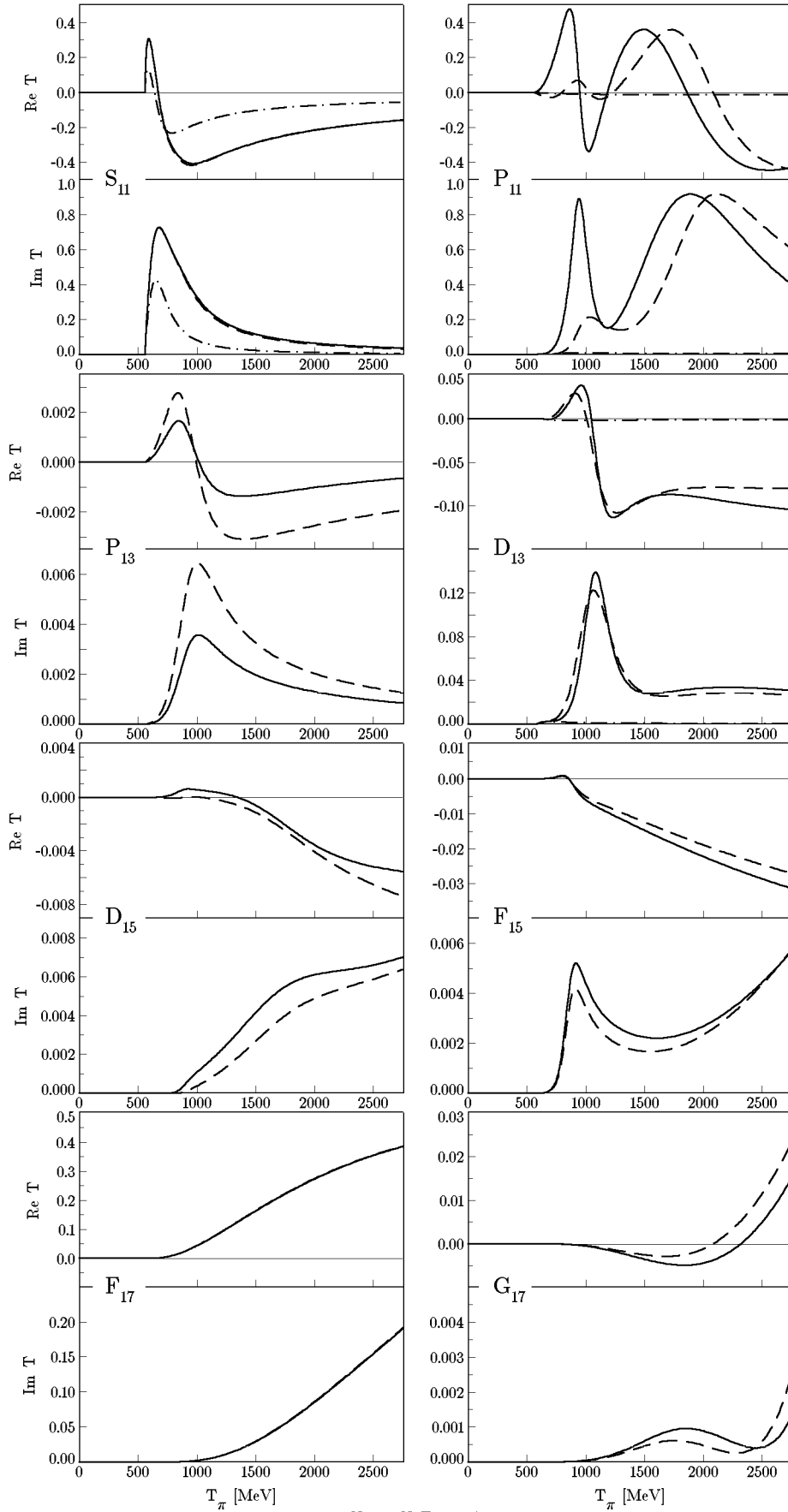
<http://arxiv.org/ps/nucl-th/9501011v2>

Fig. 4



$\pi\bar{N} \rightarrow \eta N$  T matrix :  
 (— · — ·) single resonance model,  
 (—) multiresonance unitary model with 3 resonances in P11,  
 (— —) multiresonance unitary model with 4 resonances in P11.

Fig. 5

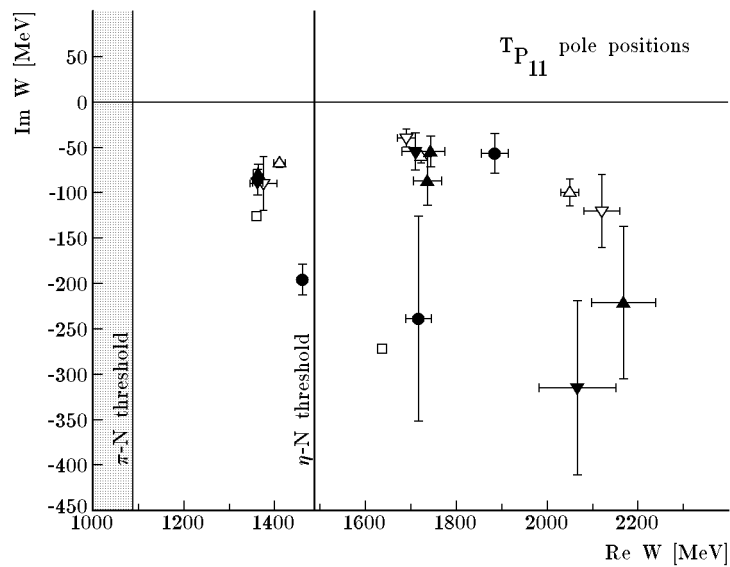


$\eta N \rightarrow \eta N$  T matrix :

(- · - ·) single resonance model,

(—) multiresonance unitary model with 3 resonances in  $P_{11}$ ,

(- -) multiresonance unitary model with 4 resonances in  $P_{11}$ .

**Fig. 6**

- $\nabla$  CMU-LBL PWA [15, 16]
- $\triangle$  K-H PWA (  $M - i \Gamma/2$  ) [17]
- $\bullet$  Manley and Saleski (  $M - i \Gamma/2$  ) [25]
- $\square$  Arndt et al. solution SM90 [29]
- $\blacktriangledown$  Our solution with 3 resonances
- $\blacktriangle$  Our solution with 4 resonances